

PIV Study of In-Cylinder Confined Swirling Flow for Scavenging 2-Stroke Marine Diesel Engines

S. Haider¹, K.E. Meyer¹, D. Cavar¹, J. Schramm¹ and Stefan Mayer²

¹Department of Mechanical Engineering, Technical University of Denmark, Kgs. Lyngby, 2800 DENMARK.
 sdh@mek.dtu.dk

²Basic Research, MAN DIESEL, Denmark.

ABSTRACT

Stereoscopic PIV measurements are conducted to study the confined swirling flow in scavenging process for large 2-Stroke marine diesel engines. The measurements are conducted at two different Reynolds numbers and 6 measuring planes along the length of a simplified scaled model of an engine cylinder. The results show a decaying helical swirling flow with recirculating core. Tangential velocity profile resembles 'Rankine vortex' and axial velocity shows a wake like profile behaviour.

1. INTRODUCTION

Turbulent swirling flow is one of the complex flows that exist in many engineering applications, such as aircraft gas combustors, pulverized coal burners, turbo machinery, cyclone separators, centrifugal gas separators and large-scale pipeline systems. Large two-stroke diesel engines, specifically the low speed engine (LSE) type, are employed with uniflow scavenging method for higher engine thermal efficiency due to better air/gas exchange (Pevzner, Leonid A., 1998). Fresh air enters the cylinder through in-take ports on the cylinder liner close to the bottom dead centre (BDC) and the exhaust gases are removed through single exhaust port in cylinder head. The scavenging ports are at an angle (15°- 25°) with the cylinder radius to impart tangential velocities and thus create a confined swirling flow removing the exhaust gases from the cylinder, providing the fresh air charge for the next cycle and enhancing mixing of the injected fuel and its consequent combustion. This makes scavenging a very important process to be investigated and optimized for the development of efficient engines both in terms of fuel consumption and pollution of the environment.

Compared to small two stroke diesel engines, very little experimental work is available in scientific literature focused on studying the scavenging process in uniflow-scavenged large marine diesel engines. Authors could only find the results of experiments conducted by Litke (1999) investigating the influence of inlet angles of the inlet ports on the scavenging efficiency by using liquids on a 1:4 scaled engine model instead of gases. The present work is a Stereo PIV based study of the in-cylinder confined swirling flow using air at room temperature and pressure and is a part of the project being conducted at DTU-Mechanics aimed to investigate the uniflow scavenging in LSE.

2. EXPERIMENTAL APPROACH

Large physical size of LSE makes it very difficult and expensive to conduct direct experimental investigations. Therefore, to characterize this flow, an experimental down-scale and

simplified model of the engine cylinder is developed. An overview of the experimental setup is shown in figure 1. The scavenging flow test rig is connected with a fan with speed controller and an orifice meter to measure the volumetric flow rate through the setup.

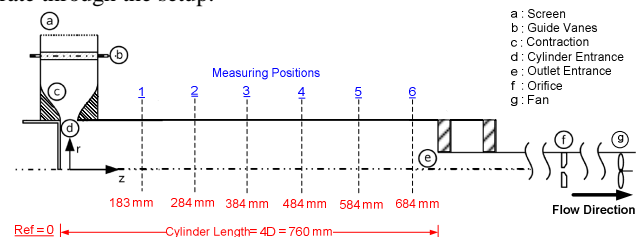


Figure 1. Scavenging Flow Test rig

2.1 Cylinder

A transparent acrylic cylinder (produced using casting process to give good optical properties) is used. The total length of the cylinder is (L=1945 mm) with internal diameter ($D_i=190$ mm) and external diameter ($D_o=200$ mm). However, for the current study, the cylinder length is kept at 4D i.e. equal to the stroke-to-bore ratio for LSE. The inlet section (Figure 2) is fitted on one end of the cylinder, while the outlet section is fitted on the opposite side.

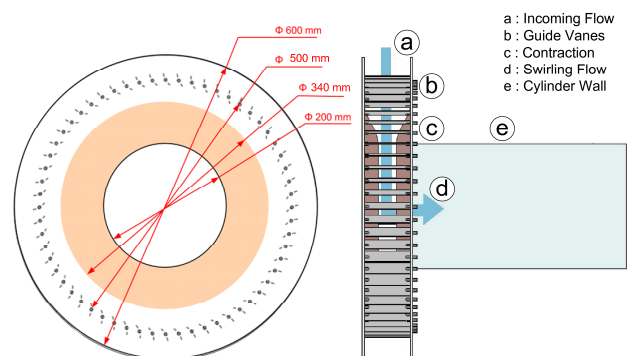


Figure 2. Inlet Section

2.2 Inlet-Section

The inlet section (Figure 2) consists of two transparent ring-shaped acrylic plates ($D_o=600$ mm). The plates are fitted in parallel by mounting 60 guide vanes in between them thus serving as walls. The distance between the internal walls of the plates and height of the individual blade is 100 mm. A screen with 51% open-area ratio is glued around the outer periphery of

the inlet section as shown in Figure 1. Flow enters the inlet section in radial direction while guiding vanes divert the flow at the targeted angle. The guide vanes are adjustable in order to provide a desired degree of swirl to the flow. For this study, guide vanes are adjusted in a way that flow enters the cylinder at an angle of 20° with the radius. The guiding vanes are mounted at a large radial distance of 500 mm from the geometric centre of the cylinder and close to the inlet (Figure 2). This will give some time to the flow after the vanes to settle thereby minimizing the wake effects. Further, before entering into the cylinder the flow enters a bell-mouth shape contraction section which will accelerate the flow and reduce the velocity fluctuations and diminish the turbulence levels. The acrylic cylinder is entered in to the inlet section from one side and from the other side, a transparent piston is mounted. The piston can slide inside the cylinder thus partially/ fully closing the cylinder inlet section, similar to real engine where the piston uncovers and covers the scavenging ports during the scavenging process. However, the current work is focused on studying the swirling flow when the piston is at the BDC and therefore the inlet to the cylinder is kept fully open.

2.3 Outlet Section

The outlet section (Figure 1) consists of a smaller diameter pipe ($d_o=110$ mm) with length of $l=1415$ mm. The chosen large pipe length is aimed to minimize any possible effect on the nature of the swirling flow inside the cylinder, which might come from bending of the pipes connecting the setup to orifice and fan at the outlet section end. The shape of the outlet provides a flat-bottom head to the cylinder. The outlet section can slide inside the cylinder thereby providing the experiments with a desired effective cylinder length.

3. STEREOSCOPIC PIV SETUP

An overview of the Stereoscopic PIV setup is given in Figure 3. The test rig is mounted on a table which is aligned in parallel with an electronically controlled traverse system. The laser cavity and two cameras are fitted on the traverse system.

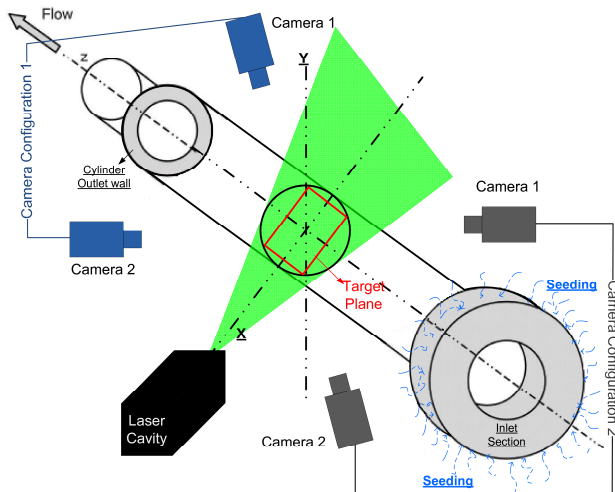


Figure 3. Stereoscopic PIV Setup

3.1 Alignment and Calibration

The NewWave Solo Nd:Yag pulse laser device (120 mJ pulses @ 15 Hz, Wavelength 532 nm) is mounted on the traverse mechanism in a way that the laser sheet is perpendicular to the

cylinder. The laser sheet is aligned with the laser light reflected from the cylinder wall. This ensures that the laser sheet is perpendicular to the cylinder. Two Dantec HiSense cameras with 1344×1024 pixels are equipped with 60 mm focal length lens and a green light filter. Both cameras, mounted on the same traverse system are at one side of the laser sheet while the cylinder is placed in between the two cameras (Figure 3). The calibration target was attached on a disc of the same diameter as the internal diameter of the cylinder. The calibration target can then slide inside the cylinder and is kept aligned with the laser sheet at one of the measuring positions. The cameras were focused on a rectangular target plane within the pipe diameter, avoiding the cylinder wall. Calibration was performed using 3rd Order XYZ-Polynomial Imaging model in Dantec DynamicStudio software. In addition, the disparity error correction, provided in the software, is also performed.

In order to capture all the measuring positions, two configurations are used for positioning the cameras (Figure 3). Due to view angle issues, camera positioning configuration 1 cannot view the measuring positions near the outlet and thus configuration 2 is used. Calibration process is repeated for configuration 2. For the camera receiving the forward scatter laser light, the F-number is set to 5.6 and for the other camera receiving the backward scatter, F-number is 4. Laser cavity and cameras are mounted on the same traverse system with their positions fixed relative to each other. For each configuration, calibration is performed at single measuring position and then the traverse system is moved in axial direction (Z-axis) to other measuring planes.

3.2 Seeding

The seed generator contains 75/25 % by volume glycerol-Water solution. The size distribution of seeding droplets is in range of 1-3 μm . In order to obtain an adequate uniform seeding, the particles should mix properly with the incoming air entering the inlet section. For this purpose a metal frame (diameter 860 mm and width 150 mm) is mounted around the inlet section. A plastic pipe (diameter 40 mm) is tied with the internal periphery of the metal frame in a helical shape so as to cover the whole breadth of the metal frame and consequently the inlet surface. A lot of small holes are drilled in the pipe wall facing the inlet of the experimental setup. The two ends of the pipe are connected to the seed generator. The radial distance of the pipe wall from the inlet surface is sufficiently large not to affect the incoming flow and provides a uniform seeding across the inlet surface.

3.3 Data Acquisition

PIV data acquisition, is performed at two Reynolds numbers ($Re_A=0.99 \times 10^5$ and $Re_B=1.15 \times 10^5$) based on the average axial velocity. For each Re , measurements are conducted at 6 cross sectional planes along the length of the cylinder, with their distance measured from the piston surface as reference (Figure 1). At every position and a given Re , 994 PIV snapshots are taken and data analysis is performed using Dantec DynamicStudio software. Static pressure at the cylinder wall is also measured for every measuring position at both Re using a differential micro-manometer.

4. RESULTS

4.1 Mean Velocity Data

The experimental data shows that despite axis-symmetric geometry of the whole experimental setup (the test cylinder and

inlet section in particular), the resulting in-cylinder confined swirling flow is comprised of a ‘helical vortex’. At both Re , the core of the vortex is not coinciding with the geometric centre of the cylinder for all 6 positions along the cylinder length. The radial distance of the core from the geometric centre is not constant at all measuring positions and pitch of the helix is longer than the 4D length of the cylinder, as it does not complete one revolution from inlet to outlet.

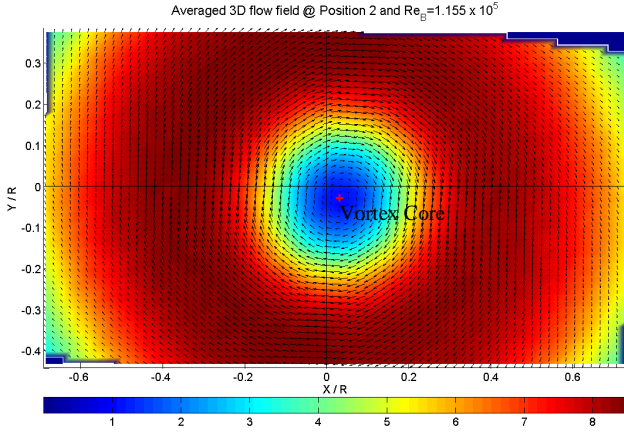


Figure 4. Averaged 3D Velocity Field (Contour = U_z)

For all measuring positions, the averaged 3D velocity field show a high velocity region between a slow moving core and near wall region (Figure 4). The mean tangential velocity U_θ profiles show ‘Rankine Vortex’ behaviour with an inner ‘forced vortex’ region and an outer ‘free vortex’ region (Figure 5). The size of the free vortex core increases along the flow direction i.e. from measuring position close to the cylinder inlet to position near cylinder outlet and shrinks again as the flow approaches the cylinder outlet which is smaller in diameter than the test cylinder. The magnitude of mean axial velocity U_z is higher than tangential velocity and generates a wake-like profile without counter flow.

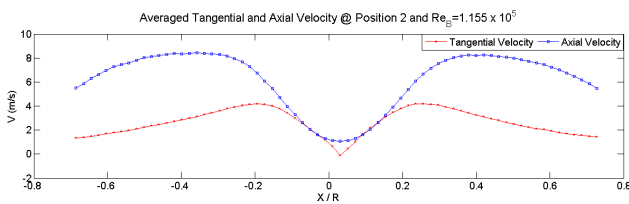


Figure 5. Tangential and Axial Velocity at $Y=0$

With R and R_o as local and internal radius of the cylinder respectively, the local swirl number distribution is calculated using equation (1) [3]

$$S = \frac{(U_z U_\theta) R}{\left(U_z^2 - \frac{U_\theta^2}{2} \right) R_o} \quad (1)$$

As it can be seen from (Figure 6), the magnitude of axial velocity is higher than the tangential velocity. This indicates the low swirl number flow. The local swirl number distribution (Figure 6) shows a sharp gradient in the core region attaining a maximum value and then declining as the radial distance

increases followed by a gradual increase at larger radial distances. For all the measuring positions, the velocity magnitude and swirl intensity decrease along the flow direction. The type of swirl flow can thus be defined as ‘Decaying Swirl Flow’ type [4].

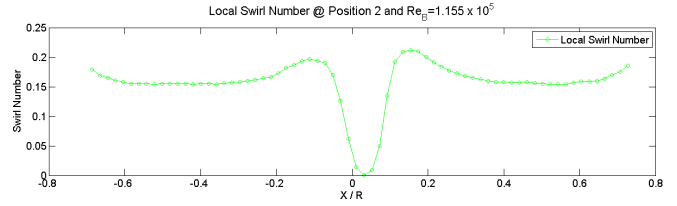


Figure 6. Local Swirl Number Distribution at $Y=0$

For Re_A and Re_B , at all measuring planes, Figure 8 and 9 give an overview of U_θ and U_z profiles (presented along X-axis and at $Y=0$) non-dimensionalized with magnitude of Mean velocity V_{mean} calculated along the same line for that particular reading.

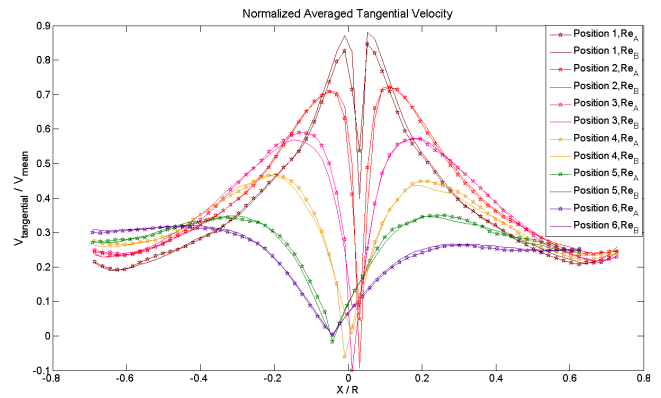


Figure 7. Non-Dimensionalized U_θ at $Y=0$

The U_θ profile shape does not change with increasing Re and the variation in magnitude is observed only in the forced vortex core region, for measuring positions near cylinder inlet. The U_θ profile becomes fuller along the flow from inlet to outlet.

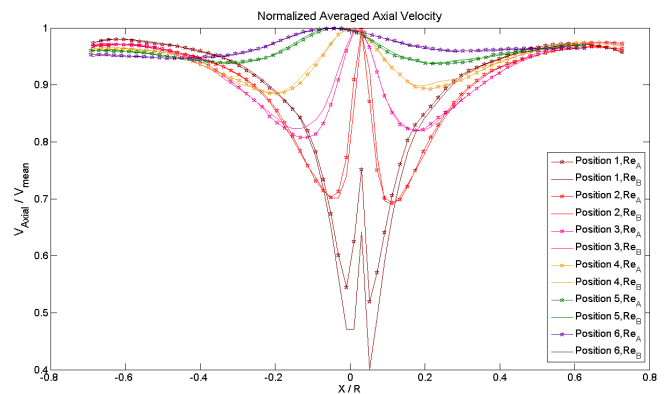


Figure 8. Non-Dimensionalized U_z at $Y=0$

For U_z like U_θ , Re does not significantly affects magnitude and shape of the profiles except in the core and transition region.

The non-dimensionalized U_z profiles, however, provide additional information in understanding the contribution of tangential and axial velocity components to the mean velocity V_{mean} at different spatial positions in the cross-sectional plane. U_z seems to be dominant in the core region and at larger radial distances whereas U_θ contributes more in the transition region and near-wall radial positions. In general, the overall effect of Re is only seen in terms of intensity whereas the velocity profiles and distributions remain unchanged. Due to the helical vortex, at all measuring positions, the minimum values of U_θ and maximum values of U_z have an offset from (X/R=0).

The vorticity plot (Figure 9) shows a high vortical core region. The vorticity decreases along radius as the transition from 'forced vortex' to free vortex occurs. However, the transition region attains zero or minimum vorticity values and appears like a non-vortical ring in between forced and free vortices. The vorticity distribution becomes uniform along the main flow as the tangential velocity profile becomes fuller and swirl intensity decays.

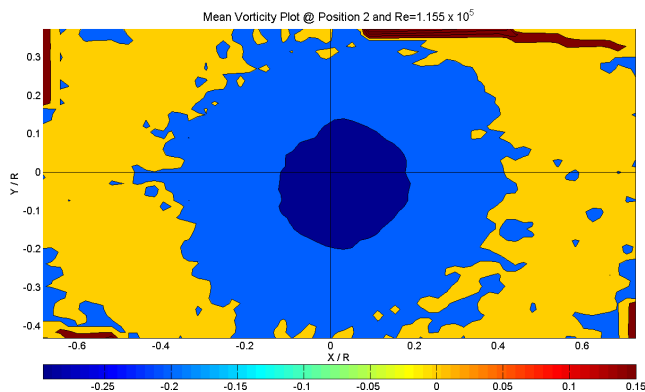


Figure 9. Averaged Vorticity (1/s)

4.2 Instantaneous Velocity Data

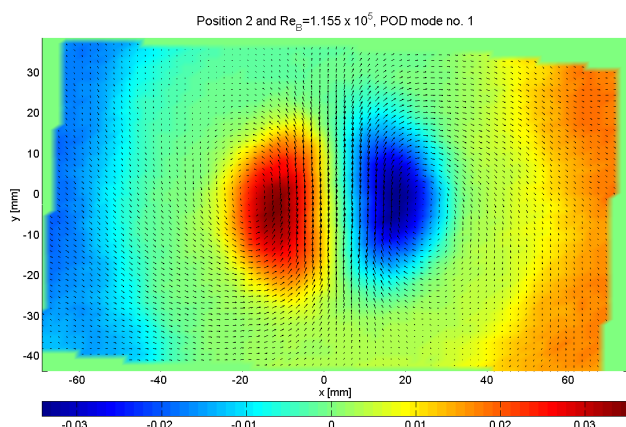


Figure 10. POD mode 1 with 11% Energy

Snapshot based Proper Orthogonal Decomposition (POD) analysis [5] show that the most energetic modes have the shape of a pair of counter rotating vortices, see figures 10 and 11 (contour shows out of plane velocity component). In a reconstruction, the modes have to be added to the mean flow

shown in figure 4 using a reconstruction coefficient found by projecting the snapshot onto the POD mode. The effect of adding one of the POD modes to the mean field is to displace the core of the vortex seen in the mean field. Using both modes, all practical positions of the vortex core can be reconstructed. Analysis of the reconstruction coefficients therefore provides statistics on the movement of the vortex core.

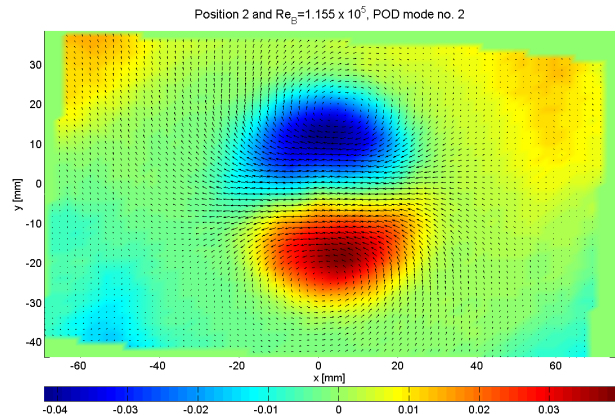


Figure 11. POD mode 2 with 8.25% energy

5. CONCLUSIONS

The flow is a helical swirling flow with core recirculation. The tangential and axial velocities show a Rankine vortex and wake-like profiles respectively and their magnitudes decrease along the flow with profiles becoming gradually fuller. With small variation only in the forced vortex core and transition region, an increase in Re seems to have no effect on the flow characteristics. Low swirl number shows a dominant axial momentum. The vortex core is the mostly pronounced vortical region in the flow. However, vorticity distribution becomes uniform as the flow decays and sharp velocity gradients are minimized.

ACKNOWLEDGMENTS

Authors acknowledge MAN DIESEL and Danish Centre for Maritime Technology (DCMT) for funding the current project.

REFERENCES

- [1] Pevzner, Leonid A. (1998) Aspects of marine low-speed, cross-head diesel engine lubrication. *Lubrication Engineering*, **54**(6), 16-21.
- [2] Benedykt Litke (1999) The influence of inlet angles in inlet ports on the scavenging process in two-stroke uniflow-scavenged engine, *Trans. The built Environment, Marine Technology III*, **45**, 247-252.
- [3] Ribeiro M. M. and Whitelaw J. H. (1980) Coaxial Jets With and without swirl. *Journal of Fluid Mechanics*, **96**(4), 769-795.
- [4] Martemianov S. and Okulov V.L. (2004) On heat transfer enhancement in swirl pipe flows, *International Journal of Heat and Mass Transfer*, **47**, 2379-2393.
- [5] L. Sirovich (1987. Turbulence and the dynamics of coherent structures. Part I: Coherent structures. *Quart. Appl. Math.*, **45**(3):561-571.